Materials and Structures (2014) 47:293–310
DOI 10.1617/s11527-013-0061-1

ORIGINAL ARTICLE

Behaviour of recycled aggregate concrete filled stainless steel stub columns

Vivian W. Y. Tam · Zhi-Bin Wang · Zhong Tao

Received: 23 March 2012 / Accepted: 18 March 2013 / Published online: 26 March 2013

Abstract Past research indicates that recycled aggregate concrete (RAC) could be successfully used in concrete-filled steel tubular (CFST) columns. Their yielded performance is almost as good as that of the traditional CFST columns. In addition, as a comparatively new construction material, stainless steel can be used to replace carbon steel for enhancing the durability and ductility of CFST columns. With an aim to combine the advantages of both RAC and stainless steel, RAC is proposed in this paper to be used as a filling material for stainless steel tubes. A test program is introduced in this paper to investigate the behaviour of RAC-filled stainless steel stub columns. For comparison purposes, reference specimens with carbon steel tubes are also tested. In the end, finite element analysis is conducted to simulate the current test results and those reported in the literature.

Keywords Concrete-filled steel tubes · Stainless steel · Recycled aggregate concrete · Axial compression · Nonlinear analysis · Strength

List of symbols

A_c	Cross-sectional area of concrete (mm^2)
A_s	Cross-sectional area of steel (mm^2)
B	Width of the square or rectangular steel tube (mm)
D	Diameter of the circular steel tube or depth of the rectangular steel tube (mm)
E_c	Elastic modulus of concrete (N/mm^2)
E_{sc}	Initial elastic modulus of the composite column (N/mm^2)
f'_c	Cylinder compressive strength of concrete (N/mm^2)
f_{ck}	Characteristic concrete strength (=$0.67f_{cu}$ for normal strength of concrete, N/mm^2)
f_{cu}	Compressive cube strength of concrete (N/mm^2)
f_y	Yield strength of steel (N/mm^2)
L	Specimen length (mm)
N	Axial load (kN)
N_{EC4}	Predicted ultimate strength using Eurocode 4 (kN)
N_{uc}	FE predicted ultimate strength (kN)

V. W. Y. Tam
School of Computing, Engineering and Mathematics, University of Western Sydney, Penrith, NSW 2751, Australia

Z.-B. Wang
College of Civil Engineering, Fuzhou University, Fuzhou 350108, Fujian, China

Z.-B. Wang
Department of Civil Engineering, Tsinghua University, Beijing 100084, China

Z. Tao (✉)
Institute for Infrastructure Engineering, University of Western Sydney, Penrith, NSW 2751, Australia
e-mail: z.tao@uws.edu.au

N_{ue} Ultimate strength of the column (kN)
γ Recycled aggregate replacement ratio (−)
SI Ratio of the compressive strength of a RACFST column to that of its reference normal CFST column (−)
t Wall thickness of the steel tube (mm)
ε Strain (10^{-6})
ε_{ue} Axial strain at the peak load (10^{-6})
σ Stress (N/mm^2)
ξ Confinement factor (−)

1 Introduction

Recycled aggregate concrete (RAC) may be recognised as a type of green material which can help conserve the natural resource, decrease energy consumption, reduce landfill requirements and save construction cost [1]. However, some widely recognised drawbacks of RAC, such as low strength, low elastic modulus, high creep and shrinkage, have limited its development and structural applications. Against this background, Konno et al. [2] first recommended to use steel tubes confining RAC with an aim to improve the strength and stiffness of RAC. Another advantage of this construction is that the tube can avoid the moisture loss, which helps to reduce the shrinkage and creep of RAC. The confinement idea was further explored by Yang and Han [3], and the concept of recycled aggregate concrete filled steel tubes (RACFST) was then put forward.

In investigating the confinement of steel tubes on RAC, experimental studies were first carried out by Konno et al. [2, 4] to investigate the axial compression behaviour of six circular stub columns, in which the concrete was made with 100 % of recycled coarse aggregate. To maximise the confinement, the axial load was only applied to the concrete through a loading plate. It was found that the ultimate strength of specimens with RAC was almost the same as that of reference specimens with normal concrete. However, stiffness of the former was smaller than that of the reference specimens.

Apart from the research conducted by Konno et al. [2, 4], follow-up studies were carried out by other researchers on either RACFST columns or steel tube confined RAC columns [3, 5–14].

Yang and Han [3, 5] studied the performance of RACFST stub columns, beams and beam-columns with circular and square sections under short-term static loading. The recycled aggregate replacement ratio (γ) was chosen to be 25 or 50 %. It was found that the mechanical behaviour of the RACFST specimens is similar to that of concrete filled steel tubular (CFST) specimens with ordinary concrete, but the modulus and strength of the former are slightly lower than those of the latter. For the RACFST stub columns, the strength reduction was 1–9.4 %, whilst the strength decrease was found to be 3.5 to 8.1 % for the RACFST beams and 1.7 to 13.5 % for the RACFST beam-columns.

Yang et al. [6] reported that concrete shrinkage and creep strains of RACFST stub columns are about 6 to 23 % higher than those of CFST stub columns with normal concrete. A mechanical model was developed in [13] to consider the influence of long-term sustained loading on the load-carrying capacity of the RACFST columns, where the influence of γ was considered. A formula to predict the strength reduction of RACFST columns was proposed incorporating the influence of long-term loading.

Yang and Zhu [7] and Yang et al. [8] carried out studies on the cyclic behaviour of RACFST beam-columns. The studies further confirmed that the strength and stiffness of the RACFST specimens are slightly lower than those of the specimens with normal concrete, but fibre element models developed for normal CFST columns can still be used to simulate the behaviour of the RACFST specimens.

On the contrary to previous findings, Mohanraj et al. [11] reported test results of 4 axially loaded RACFST columns, and an average strength increase of 3.9 % was found for the RACFST specimens compared with specimens with normal concrete. The slenderness ratios (L/D, or L/B) of the specimens ranged from 3.9 to 12.5, where L is the effective buckling length of a specimen, D is the overall diameter of the circular tube and B is the overall width of the square tube. In making the RAC, 25 % natural coarse aggregate was replaced by recycled coarse aggregate. The mix design and production of recycled aggregate were not introduced in this paper. The measured concrete cube strengths (f_{cu}) for normal concrete and RAC were 25.03 N/mm^2 and 28.14 N/mm^2, respectively. As can be seen, the strength increase was 12.4 % for RAC when compared with the reference normal concrete, which was not explained by Mohanraj et al. [11].

Chen et al. [9, 10] carried out a series of tests on circular and square RACFST stub columns with γ

values varied from 10 to 100 %. They found a slightly increase in load-carrying capacity when RAC was used to replace normal concrete. Generally, the concrete strength increased with increasing γ, and so was the load-carrying capacity of the CFST column. The average strength increase was about 7 % for RAC with different γ values when compared with normal concrete, whilst the average load-carrying capacity for all RACFST columns was approximately 5 % higher than that of the normal CFST columns. Similar phenomenon was also observed by Shi et al. [12] who conducted axial compression tests on sixteen RACFST stub columns and two reference CFST stub columns. For normal concrete in [12], the measured concrete strength f_{cu} was 42.6 N/mm^2, whilst those for RAC with a γ value of 25, 50 and 75 % were 43.4 N/mm^2, 43.9 N/mm^2 and 45.6 N/mm^2, respectively. For the RAC with a γ value of 100 %, however, a considerable strength decrease was found and f_{cu} was only 35.9 N/mm^2.

It is widely believed that RAC has a slightly lower compressive strength compared with a control mix made with original aggregate [1]. To achieve the same or higher compressive strength as conventional concrete, RAC can be made with lower water-cement ratio or adding more cement content [15]. It was mentioned by Chen et al. [9, 10] that both natural coarse aggregate and recycled coarse aggregate used were cleaned and dried. In general, water absorption capacity of the dried recycled coarse aggregate is higher than that of natural coarse aggregate [1]. If a same mix is used in preparing RAC and normal concrete with no additional water is added to compensate for the water absorbed by the dried recycled aggregate, the effective water-cement ratio achieved for the RAC will thus be lower than that of normal concrete. This may explain the strength increase of RAC observed by Chen et al. [9, 10], Mohanraj et al. [11], and Shi et al. [12].

More recently, Xiao et al. [14] reported test results of 12 steel tube confined RAC short specimens under axial compression. Continuous strength decrease was found when γ increased from 0 to 70 %. An average strength decrease of 13.2 % was found for steel tube confined RAC specimens with a γ value of 70 % when compared with specimens with normal concrete. The strengths, however, were very close for steel tube confined RAC specimens with γ values of 70 and 100 %. Meanwhile, it was found that steel tube confined RAC specimens had higher peak strains than specimens with normal concrete, and the increase in the peak strain varied from 33.7 to 49.3 %.

The above literature review indicates that past studies were mainly focused on RAC-filled carbon steel columns, and laboratory-made recycled aggregate was normally used. Till now, no research has been conducted on RACFST columns with stainless steel. In fact, as a comparatively new construction material, stainless steel can be used to replace carbon steel for enhancing the durability and ductility of CFST columns [16]. Therefore, RAC is proposed in this paper to be used as a filling material for stainless steel tubes. This kind of composite columns is expected to successfully combine the advantages of both stainless steel and RAC.

Against the above research background, a test program is introduced in this paper to investigate the behaviour of RAC-filled stainless steel stub columns under axial compression, where commercially produced recycled aggregate is used. Finite element analysis is then carried out to simulate the test results.

2 Experimental investigation

2.1 General

A total of 16 stub columns were prepared, including twelve RACFST specimens and four reference CFST columns with normal concrete. Two types of cross-sections (circular and rectangular), as shown in Fig. 1, were tested, where D is the diameter of the circular tube or depth of the rectangular tube, and B is the width of the rectangular tube. The height (L) of all columns is taken three times the diameter (D) of the circular section or the depth (D) of the rectangular section. The main parameters considered in this study are: (1) cross-section shape (circular, rectangular); (2) steel type (carbon steel, stainless steel); and (3) recycled aggregate replacement ratio γ (0, 25, 50, 100 %).

Table 1 provides the specimen details, where specimen designations starting with a C or R refer to specimens with circular or rectangular cross-sections, and the following letter C or S indicates that carbon steel or stainless steel was used. The numbers of 0, 25, 50 and 100 in the specimen labels denote RACFST columns with a γ value of 0, 25, 50 and 100 %, respectively.

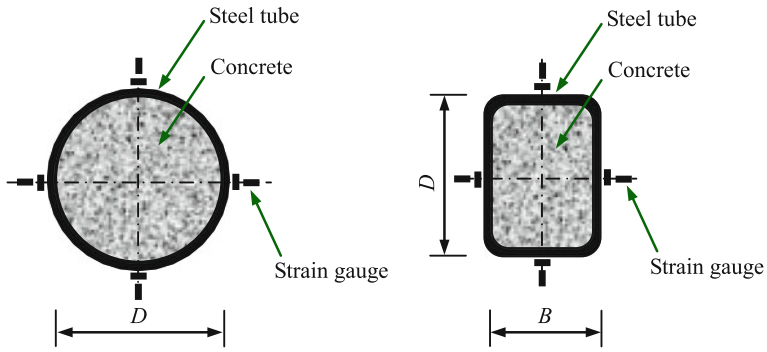

Fig. 1 Cross-sections of the test specimens

Table 1 Details of the specimens and test results

Specimen type	No.	Label	D (mm)	B (mm)	t (mm)	L (mm)	γ (%)	f'_c (N/mm^2)	ε_{ue} (με)	E_{sc} (N/mm^2)	N_{ue} (kN)	SI	N_{uc} (kN)	N_{ue}/N_{uc}	N_{ue}/N_{EC4}
Circular	1	CC-0	139.1	–	2.79	420	0	41.2	13,494	40,440	1,211.6	–	1,247.1	0.972	0.979
	2	CC-25	138.6	–	2.79	420	25	41.7	15,453	38,860	1,175.1	0.970	1,251.9	0.939	0.950
	3	CC-50	138.7	–	2.79	420	50	41.0	14,526	37,640	1,212.5	1.001	1,244.7	0.974	0.986
	4	CC-100	138.0	–	2.79	420	100	37.8	12,368	36,110	1,147.5	0.947	1,208.6	0.949	0.974
	5	CS-0	168.9	–	2.86	510	0	41.2	10,521	35,100	1,707.5	–	1,655.8	1.031	1.075
	6	CS-25	168.4	–	2.86	510	25	41.7	10,099	35,030	1,595.1	0.934	1,663.8	0.959	1.003
	7	CS-50	169.7	–	2.86	510	50	41.0	8,658	33,040	1,607.4	0.941	1,664.1	0.966	1.006
	8	CS-100	170.6	–	2.86	510	100	37.8	11,227	28,950	1,573.1	0.921	1,608.9	0.978	1.016
Rectangular	9	RC-0	197.8	98.5	3.83	600	0	41.2	3,675	47,810	1,612.8	–	1,718.6	0.938	0.920
	10	RC-25	199.8	99.9	3.83	600	25	41.7	3,878	43,320	1,609.5	0.998	1,724.7	0.933	0.897
	11	RC-50	199.4	99.2	3.83	600	50	41.0	3,939	42,390	1,608.2	0.997	1,713.2	0.939	0.909
	12	RC-100	200.0	98.7	3.83	600	100	37.8	3,209	39,150	1,567.0	0.972	1,650.2	0.950	0.914
	13	RS-0	200.7	97.1	3.96	600	0	41.2	3,054	42,890	1,422.9	–	1,418.5	1.003	1.021
	14	RS-25	200.2	98.5	3.96	600	25	41.7	3,101	40,410	1,350.2	0.949	1,426.3	0.947	0.955
	15	RS-50	200.7	97.9	3.96	600	50	41.0	4,032	39,460	1,388.7	0.976	1,414.3	0.982	0.993
	16	RS-100	200.2	98.9	3.96	600	100	37.8	3,449	34,820	1,291.8	0.908	1,360.3	0.950	0.956

2.2 Material properties

Both mild steel and austenitic stainless steel (grade 304) were used, and coupon tests were carried out to obtain their tensile properties. For the rectangular steel tubes, all coupons were cut from the flat surfaces. Typical tensile stress–strain curves of steels are presented in Fig. 2. As can be seen, the stress–strain curve of the stainless steel shows much more significant nonlinear characteristics than that of the carbon steel. The measured tensile properties for all steels with different thicknesses (t) are given in Table 2.

Both natural and recycled coarse aggregates used in the current test program were commercially available. Compared with recycled aggregate made in a laboratory situation, commercial recycled aggregate is often mixed with some other building materials. For the current recycled coarse aggregate used, it included a small amount of tiles and bricks (less than 10 %). Same mix proportions were used for all concrete: (1) cement: 465 kg/m^3; (2) water: 215 kg/m^3; (3) sand: 691 kg/m^3; (4) coarse aggregate: 1,021 kg/m^3; and (5) water reducer: 4,430 ml/m^3. The recycled coarse aggregate replacement ratios γ are determined to be

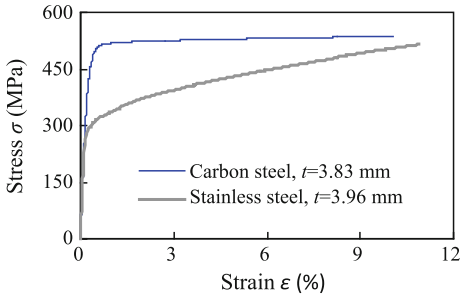

Fig. 2 Typical measured stress–strain curves for steel

0, 25, 50 and 100 %. When γ is 0 %, the concrete is virtually normal concrete without recycled coarse aggregate being used. It is worth noting that recycled fine aggregate was not used in RACFST specimens in previous studies. This is owing to the fact that recycled fine aggregate has much higher adhered mortar content than recycled coarse aggregate. Therefore, the use of recycled fine aggregate tends to be associated with much more significant adverse effects on the structural behaviour of concrete [1]. Following the previous work in this area, recycled fine aggregate is not used in the current study.

Concrete cylinders were prepared and tested to determine compressive strength (f_c') and elastic modulus (E_c) of concrete. The measured properties of different batches of concrete are presented in Table 3. At 7 and 28 days, the concrete strength and elastic modulus slightly dropped with the increase of the γ value. A same trend is found for the density of the RAC measured at 28 days. At the time of testing (about 7 weeks), however, the concrete strength of RAC with a γ of 25 or 50 % is quite close to that of the normal concrete. For the RAC with a γ of 100 %, the final measured strength f_c' is 8.3 % lower than that of normal concrete.

2.3 Specimen preparation

Cold-formed hollow steel tubes were purchased and cut to the required length. Two steel end plates of 12 mm thickness were tack welded to a steel tube before filling the tube with concrete. A hole was cut on the top end plate and used for pouring the concrete. Concrete was mixed in the laboratory with a target strength of 40 N/mm^2. The concrete was filled in layers and compacted by a vibrator. The specimens were then left to cure in the laboratory environment at room temperature. A small amount of longitudinal shrinkage occurred at the top of specimens during concrete curing. Prior to testing, high-strength plaster was used to fill this longitudinal gap, the concrete surface was then flushed with the steel tube at the top.

2.4 Instrumentation and test setup

All compression tests were performed by using an Instron testing machine as shown in Fig. 3. Four axial

Table 2 Material properties of steel

Steel type	Thickness t (mm)	Elastic modulus (N/mm^2)	0.2 % proof stress f_y (N/mm^2)	Stain-hardening exponent	Possion's ratio	Yield strain (10^{-6})	Ultimate strength (N/mm^2)	Elongation percentage (%)
Stainless, circular tube	2.86	196,300	339.6	8	0.293	3,909	770.6	71.3
Stainless, rectangular tube	3.96	207,500	301.5	10	0.285	3,513	671.1	63.3
Carbon, circular tube	2.79	203,800	388.5	–	0.279	3,790	459.1	42.0
Carbon, rectangular tube	3.83	196,200	480.2	–	0.268	4,205	534.4	34.3

Table 3 Material properties of concrete

Type	γ (%)	Strength at 7 days (N/mm^2)	Strength at 28 days (N/mm^2)	Strength at testing (N/mm^2)	Elastic modulus at 28 days (N/mm^2)	Density at 28 days (kg/m^3)
NC	0	26.1	39.5	41.2	23,090	2,345
RAC-I	25	25.1	37.8	41.7	22,910	2,320
RAC-II	50	24.9	37.3	41.0	22,700	2,305
RAC-III	100	23.8	36.8	37.8	22,120	2,257

and four transverse strain gauges with a length of 3 mm were attached 90° apart at the mid-height of each stub column, as shown in Fig. 1. In addition, two linear variable displacement transducers (LVDT) were placed 180° apart to measure the axial deformation. All specimens were tested under monotonic loading with a loading rate of 0.5 mm/min.

3 Experimental results and discussion

3.1 Failure mode

As expected, all the composite stub columns failed due to local buckling (see Fig. 4), which is the same as the failure mode reported by many other researchers [3]. The use of RAC or stainless steel had no obvious influence on the failure pattern up to and beyond the peak load. For the rectangular stub columns, apparent lateral deformation along the minor axis developed after the peak load, as shown in Fig. 4b. This is owing to the comparatively large slenderness of the rectangular specimens along this axis.

3.2 Axial load-axial strain curves

Figure 5 demonstrates the influence of γ and cross-section shape on the axial load (N)-axial strain (ε) curves. In this paper, positive strain denotes compression and negative strain denotes tension. Considering the variation of the test results, the effect of γ on the

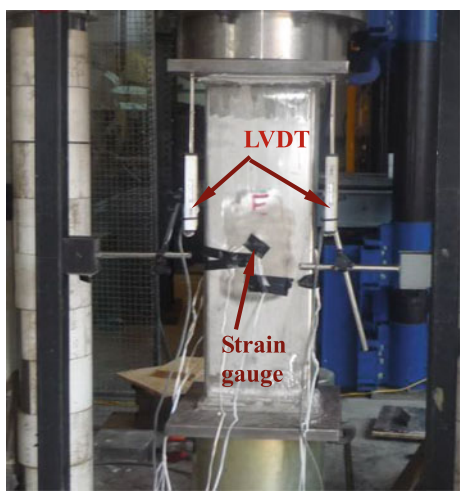

Fig. 3 Test setup for stub columns

(a) Circular specimen CS-50 **(b)** Rectangular specimen RS-100

Fig. 4 Failure appearances of typical RACFST columns after testing

shape of N–ε curves is fairly limited because the strengths and elastic moduli are quite close for RAC with different γ values, as presented in Table 3. The comparison of N–ε curves between the circular RACFST stub columns and rectangular RACFST stub columns indicates that the circular columns show much higher ductility, larger deformation ability and higher residual strength than the rectangular counterparts. This is owing to the well-known fact that a circular tube is less likely to buckle than a rectangular tube when they have close cross-section slenderness, thus the former can provide better confinement to concrete [17].

The comparison of N–ε curves between the RACFST stub columns with stainless steel and carbon steel tubes is shown in Fig. 6. Due to the different yield strengths of the carbon steel and stainless steel, the load responses in Fig. 6 are normalised with respect to the corresponding ultimate strength (N_{ue}). As can be seen, the initial portion of N/N_{ue}–ε curve of a stainless steel composite column essentially followed the curve of its corresponding carbon steel composite column before attaining the ultimate load. After that, the RACFST column with stainless steel generally displays a less steep descending branch. Owing to the strong strain hardening effect of stainless steel as shown in Fig. 2, a second ascending branch is often observed for the stainless steel composite columns. From this comparison, it can be concluded that the RACFST column with stainless steel has higher

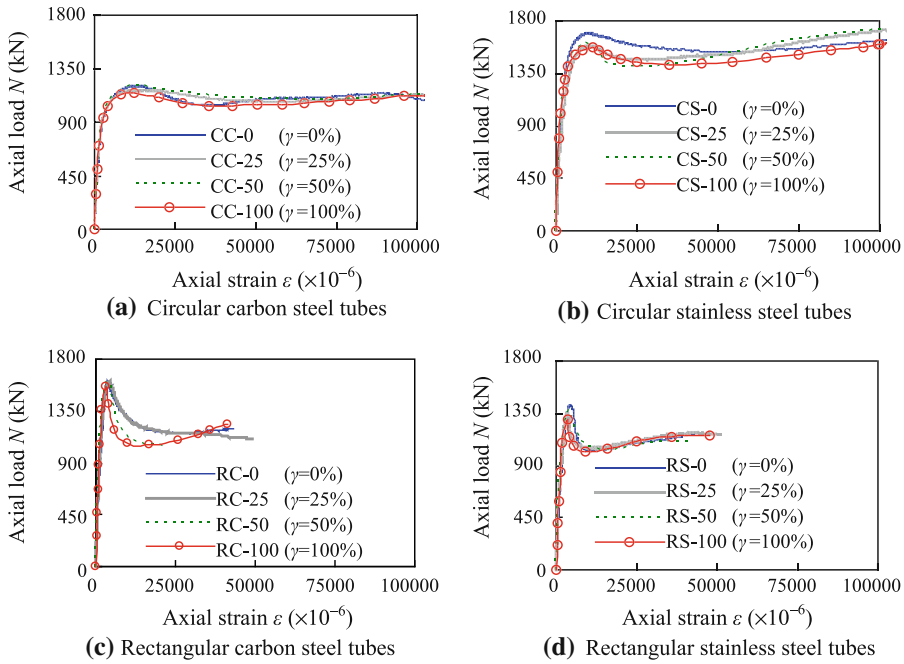

Fig. 5 Effects of γ and cross-section shape on load (N)-axial strain (ε) curves

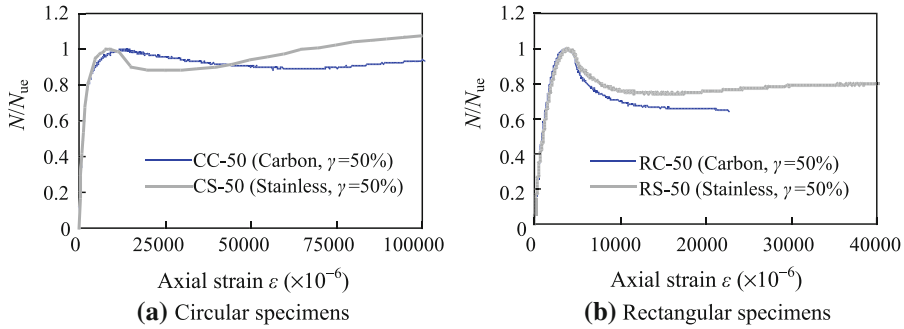

Fig. 6 Comparison of N/N_{ue}–ε curves between the stainless steel and carbon steel RACFST columns

residual strength than the counterpart with carbon steel.

3.3 Ultimate strength

The ultimate strength (N_{ue}) recorded in the tests are summarised in Table 1. In this paper, N_{ue} is simply defined as the maximum load or first peak load.

Figure 7 shows the influence of γ on N_{ue} of the RACFST specimens, in which the abbreviation NC denotes normal concrete. In general, N_{ue} decreases slightly with increasing γ. For specimens with a γ of 50 % or less, the strength decrease of the RACFST specimens is normally within 5 % compared with specimens with NC. When γ is 100 %, the strength decrease can be as high as 9.2 %. For the six RACFST specimens with carbon steel, the average strength decrease is 1.9 %, whilst the average strength decrease is 6.2 % for the six RACFST specimens with stainless steel. It seems that the replacement of normal concrete with RAC has relatively more influence on the strength of the stainless steel composite columns than on that of carbon steel specimens. This may be attributed to the fact that RAC has decreased ductility than normal concrete [18], whilst stainless steel is characterised by significant nonlinearity [19]. The decrease in ductility for RAC leads to increased strength loss after reaching its peak strength. Once the concrete confinement and/or the direct strength increase of the steel tube cannot compensate for the strength loss of concrete, peak load N_{ue} is reached for the composite column. Since stainless steel shows

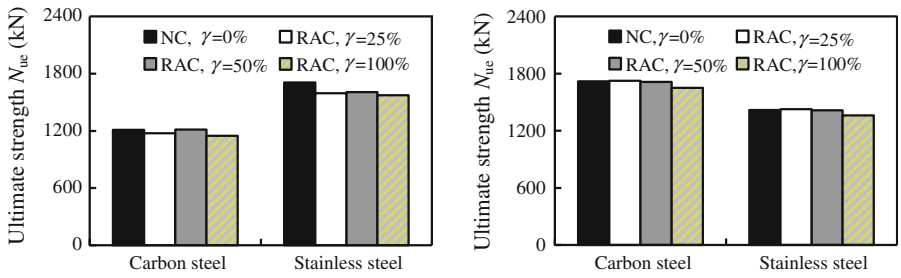

Fig. 7 Ultimate strength N_{ue} of the RACFST columns

more gradual yielding behaviour, the strength development of stainless steel is slower than that of carbon steel after reaching the proportional limit. This may explain the low strength of the RACFST columns with stainless steel. However, in general, the strength reduction of the RACFST stub columns is not very significant if the possible decline in concrete strength is considered when using RAC. This will be further explained in Sect. 4.2.

To further clarify the influence of γ on the ultimate strength of RACFST stub columns, a total of 70 test results reported by Yang and Han [3], Chen et al. [9, 10], and Shi et al. [12] are collected. The details of these test data, including geometric dimensions and material properties of the test specimens, are summarised in Tables 4 and 5. Since only cube strengths of concrete f_{cu} are reported, equivalent cylinder concrete strengths f'_c are determined according to Yu et al. [20] and presented in Tables 4 and 5. It should be mentioned that test results of 11 control specimens with normal concrete are also presented in these tables.

Figure 8a depicts the influence of γ on the concrete strength of RAC, which is normalised with the concrete strength of normal concrete. The comparison demonstrates significant variation in the compressive strength of RAC, which can be attributed to the difficulties in maintaining a uniform effective water-cement ratio in RAC [1]. This is always a concern when attempting to utilise RAC in engineering practice. Although commercial recycled aggregate was used in the present study, it involves a small amount of foreign materials, such as tiles and bricks, which has no obvious influence on the concrete strength when compared with RAC reported by others.

To quantify the influence of γ on the ultimate strength of RACFST columns, a strength index (*SI*) is defined herein, which is expressed as:

$$SI = \frac{N_{ue,RAC}}{N_{ue,NC}} \quad (1)$$

where $N_{ue,RAC}$ and $N_{ue,NC}$ are the ultimate strengths of CFST columns with RAC and normal concrete respectively. The calculated values of *SI* for RACFST columns are given in Tables 1, 4 and 5.

The influence of γ on *SI* values of RACFST columns is shown in Fig. 8b. In general, *SI* is larger than 0.9, even when γ is 100 %. A same trend is observed for the current test results. If compare the variations shown in Fig. 8a, b, it is quite interesting to note that the composite columns show a much smaller variation in compressive strength as compared with the RAC. This can be explained by two reasons: (1) only partial strength of the composite columns is contributed by the infilled concrete; and (2) the strength of RAC may be less sensitive to the influence of the effective water-cement ratio when cured in a sealed condition without moisture loss. This observation indicates the fact that the variation of concrete strength is less influential for RAC when used as a filling material in steel tubes.

3.4 Axial and lateral strains

The axial strain corresponding to the ultimate strength is referred to as ultimate strain (ε_{ue}) in this paper. Figure 9 shows the influence of γ on ε_{ue}. In general, no clear trend can be observed for the influence of γ on ε_{ue}. For a rectangular column, the value of ε_{ue} is much smaller than that of the corresponding circular column

Table 4 Independent test results of circular RACFST stub columns

No	Label	$D \times t \times L$ (mm)	γ (%)	f_y (N/mm^2)	f_{cu} (N/mm^2)	$f_c'^b$ (N/mm^2)	N_{ue} (kN)	SI	N_{uc} (kN)	N_{ue}/N_{uc}	N_{ue}/N_{EC4}
Yang and Han [3]											
1	Ca0[a]	114 × 2.19 × 342	0	335.7	42.70	35.16	741	–	677.1	1.094	1.048
2	Ca1-1	114 × 2.19 × 342	25	335.7	41.80	34.44	700	0.945	672.0	1.042	0.999
3	Ca1-2	114 × 2.19 × 342	25	335.7	41.80	34.44	711	0.960	672.0	1.058	1.015
4	Ca2-1	114 × 2.19 × 342	50	335.7	36.60	29.94	674	0.910	654.4	1.030	1.020
5	Ca2-2	114 × 2.19 × 342	50	335.7	36.60	29.94	669	0.903	654.4	1.022	1.012
6	Cb0[a]	165 × 2.57 × 495	0	343.1	42.70	35.16	1,436	–	1,295.4	1.109	1.057
7	Cb1-1	165 × 2.57 × 495	25	343.1	41.80	34.44	1,417	0.987	1,283.3	1.104	1.053
8	Cb1-2	165 × 2.57 × 495	25	343.1	41.80	34.44	1,427	0.994	1,283.3	1.112	1.061
9	Cb2-1	165 × 2.57 × 495	50	343.1	36.60	29.94	1,401	0.976	1,209.3	1.159	1.111
10	Cb2-2	165 × 2.57 × 495	50	343.1	36.60	29.94	1,402	0.976	1,209.3	1.159	1.112
11	Cc0[a]	219 × 2.86 × 657	0	350.4	42.70	35.16	2,158	–	2,138.4	1.009	0.962
12	Cc1-1	219 × 2.86 × 657	25	350.4	41.80	34.44	2,055	0.952	2,116.3	0.971	0.926
13	Cc1-2	219 × 2.86 × 657	25	350.4	41.80	34.44	2,147	0.995	2,116.3	1.015	0.968
14	Cc2-1	219 × 2.86 × 657	50	350.4	36.60	29.94	1,950	0.904	1,977.7	0.986	0.943
15	Cc2-2	219 × 2.86 × 657	50	350.4	36.60	29.94	2,014	0.933	1,977.7	1.018	0.974
Chen et al. [9]											
16	CA-0[a]	88.3 × 2.59 × 285	0	342.7	35.2	28.68	442.7	–	501.2	0.883	0.890
17	CA-1	88.2 × 2.60 × 285	10	342.7	33.0	26.70	443.9	1.003	492.1	0.902	0.910
18	CA-2	88.2 × 2.67 × 285	20	342.7	31.9	25.71	455.1	1.028	497.0	0.916	0.927
19	CA-3	88.2 × 2.55 × 285	30	342.7	36.7	30.03	478.2	1.080	501.0	0.954	0.960
20	CA-4	88.0 × 2.44 × 285	40	342.7	38.4	31.56	470.4	1.063	492.9	0.954	0.958
21	CA-5	88.2 × 2.54 × 285	50	342.7	35.7	29.13	484.9	1.095	495.3	0.979	0.984
22	CA-6	88.2 × 2.43 × 285	60	342.7	34.5	28.05	469.8	1.061	475.4	0.988	0.990
23	CA-7	88.3 × 2.54 × 285	70	342.7	40.7	33.56	474	1.071	516.1	0.918	0.920
24	CA-8	88.1 × 2.51 × 285	80	342.7	41.9	34.52	475.5	1.074	516.5	0.921	0.923
25	CA-9	88.1 × 2.40 × 285	90	342.7	39.0	32.10	469	1.059	489.8	0.958	0.957
26	CA-10	88.3 × 2.51 × 285	100	342.7	43.6	35.88	477.3	1.078	522.6	0.913	0.912
27	CB-0[a]	112.0 × 1.78 × 360	0	357.2	35.2	28.68	606.5	–	572.1	1.060	1.042
28	CB-1	112.4 × 2.07 × 360	10	357.2	33.0	26.70	607.6	1.002	598.7	1.015	0.986
29	CB-2	111.8 × 1.88 × 360	20	357.2	31.9	25.71	642.7	1.060	554.0	1.160	1.125
30	CB-3	111.7 × 1.65 × 360	30	357.2	36.7	30.03	645.5	1.064	522.3	1.236	1.133
31	CB-4	112.1 × 2.05 × 360	40	357.2	38.4	31.56	652.4	1.076	616.9	1.058	1.001
32	CB-5	112.0 × 1.90 × 360	50	357.2	35.7	29.13	630	1.039	573.4	1.099	1.040
33	CB-6	112.7 × 2.00 × 360	60	357.2	34.5	28.05	515.7	0.850	599.8	0.860	0.833
34	CB-7	112.2 × 2.01 × 360	70	357.2	40.7	33.56	609.4	1.005	615.7	0.990	0.919
35	CB-8	112.2 × 1.98 × 360	80	357.2	41.9	34.52	653.1	1.077	614.1	1.064	0.980
36	CB-9	112.1 × 1.92 × 360	90	357.2	39.0	32.10	631.7	1.042	601.1	1.051	0.995
37	CB-10	113.1 × 2.27 × 360	100	357.2	43.6	35.88	646.6	1.066	696.9	0.928	0.881
Shi et al. [12]											
38	C0-1[a]	114 × 1.74 × 397	0	300.3	42.6	35.08	650	–	573.4	1.134	1.092
39	C1-1	114 × 1.80 × 395	25	300.3	43.4	35.72	655	1.008	588.0	1.114	1.075
40	C1-2	114 × 1.80 × 401	25	300.3	43.4	35.72	651	1.002	588.0	1.107	1.071
41	C2-1	114 × 1.84 × 396	50	300.3	43.9	36.12	636	0.978	596.8	1.066	1.029

Table 4 continued

No	Label	$D \times t \times L$ (mm)	γ (%)	f_y (N/mm^2)	f_{cu} (N/mm^2)	f'_c[b] (N/mm^2)	N_{ue} (kN)	*SI*	N_{uc} (kN)	N_{ue}/N_{uc}	N_{ue}/N_{EC4}
42	C2-2	114 × 2.09 × 402	50	300.3	43.9	36.12	688	1.058	631.1	1.090	1.058
43	C3-1	114 × 2.05 × 394	75	300.3	45.6	37.48	635	0.977	636.6	0.997	0.964
44	C3-2	114 × 1.75 × 398	75	300.3	45.6	37.48	639	0.983	595.1	1.074	1.034
45	C4-1	114 × 1.71 × 400	100	300.3	35.9	29.31	557	0.857	523.8	1.063	1.035
46	C4-2	114 × 1.70 × 401	100	300.3	35.9	29.31	557	0.857	523.7	1.064	1.038

[a] Reference stub columns with normal concrete

[b] Converted from f_{cu}

due to the occurrence of earlier local buckling of the rectangular tube. Meanwhile, the carbon steel columns normally have larger ε_{ue} than stainless steel columns. This is due to the slow strength development of stainless steel as explained before.

It is found that the replacement ratio (γ) of recycled aggregate has virtually no influence on the development of lateral strains. However, some minor influence of the steel type is observed as shown in Fig. 10. Since strain readings are greatly affected by the earlier local buckling of rectangular tubes, only circular columns are selected herein to compare. Compared with the carbon steel CFST column, the corresponding stainless steel columns develop a smaller lateral strain at a same load level in the initial stage, which indicates that a carbon steel tube provides higher initial confinement to the concrete. But this influence is not significant and can be generally ignored, which is further confirmed by the comparison of interaction stresses between the stainless steel and carbon steel CFST columns presented by Tao et al. [21].

3.5 Elastic modulus

The elastic moduli of columns (E_{sc}) are presented in Fig. 11 and Table 1. E_{sc} decreased with increasing γ for both the carbon steel and stainless steel RACFST columns. This phenomenon has also been observed by other researchers. The average decrease in E_{sc} is 9.7 % for the current RACFST columns when compared with reference CFST columns. Owing to the high nonlinearity of stainless steel from the initial loading to the final failure, stainless steel RACFST columns generally have smaller E_{sc} than corresponding carbon steel RACFST columns, and the decrease can be up to 15 %.

4 Finite element simulation

4.1 Finite element model

For the carbon steel and stainless steel CFST stub columns with normal concrete, extensive research have been carried out in the past to develop rational finite element (FE) models [21]. However, limited numerical studies address the specific issue of simulating the behaviour of the RACFST columns [14].

Compared with the normal CFST columns, the only difference for RACFST columns is the utilisation of RAC. As mentioned earlier, under uniaxial compression, RAC generally has lower strength, lower elastic modulus, lower ductility, but higher peak strain than normal concrete [14, 22]. Therefore, some potential revisions may be required for any existing stress (σ)-strain (ε) model of normal concrete before it can be used in simulating the RACFST columns. Till now, the research on uniaxial σ–ε curves of RAC is still extremely limited, not to mention triaxial σ–ε curves [23]. For this reason, it is worthwhile to check the applicability of existing σ–ε models of normal concrete in simulating RACFST columns.

ABAQUS software [24] is used in this paper to conduct the FE simulation, where the concrete compression hardening/softening rule should be defined. For unconfined concrete, the uniaxial σ–ε curve can be used as the hardening/softening function. When concrete is confined laterally, an increased strength and a less steep descending branch are normally expected. The strength increase can be successfully simulated in ABAQUS through the interaction between the concrete and the steel tube in a three-dimensional model. But the increase in ductility cannot be simulated properly if the uniaxial σ–ε curve continues to be used

Table 5 Independent test results of square RACFST stub columns

No	Label	$B \times t \times L$ (mm)	γ (%)	f_y (N/mm^2)	f_{cu} (N/mm^2)	$f_c'^b$ (N/mm^2)	N_{ue} (kN)	SI	N_{uc} (kN)	N_{ue}/N_{uc}	N_{ue}/N_{EC4}
Yang and Han [3]											
1	Sa0[a]	100 × 1.94 × 300	0	388.1	42.70	35.16	666	–	604.9	1.101	1.074
2	Sa1-1	100 × 1.94 × 300	25	388.1	41.80	34.44	645	0.968	599.4	1.076	1.051
3	Sa1-2	100 × 1.94 × 300	25	388.1	41.80	34.44	660	0.991	599.4	1.101	1.076
4	Sa2-1	100 × 1.94 × 300	50	388.1	36.60	29.94	624	0.937	563.7	1.107	1.091
5	Sa2-2	100 × 1.94 × 300	50	388.1	36.60	29.94	614	0.922	563.7	1.089	1.074
6	Sb0[a]	150 × 2.94 × 450	0	344.4	42.70	35.16	1,306	–	1,293.6	1.010	0.985
7	Sb1-1	150 × 2.94 × 450	25	344.4	41.80	34.44	1,279	0.979	1,280.8	0.999	0.976
8	Sb1-2	150 × 2.94 × 450	25	344.4	41.80	34.44	1,287	0.985	1,280.8	1.005	0.982
9	Sb2-1	150 × 2.94 × 450	50	344.4	36.60	29.94	1,250	0.957	1,200	1.042	1.027
10	Sb2-2	150 × 2.94 × 450	50	344.4	36.60	29.94	1,293	0.990	1,200	1.078	1.062
11	Sc0[a]	200 × 3.73 × 600	0	330.1	42.70	35.16	2,295	–	2,211	1.038	1.011
12	Sc1-1	200 × 3.73 × 600	25	330.1	41.80	34.44	2,123	0.925	2,188.5	0.970	0.946
13	Sc1-2	200 × 3.73 × 600	25	330.1	41.80	34.44	2,238	0.975	2,188.5	1.023	0.998
14	Sc2-1	200 × 3.73 × 600	50	330.1	36.60	29.94	2,098	0.914	2,043.4	1.027	1.010
15	Sc2-2	200 × 3.73 × 600	50	330.1	36.60	29.94	2,140	0.932	2,043.4	1.047	1.031
Chen et al. [10]											
16	SA-0[a]	121 × 3.08 × 359	0	340.7	35.2	28.68	892.7	–	835.2	1.069	1.022
17	SA-1	121 × 3.25 × 359	10	340.7	33.0	26.70	915.9	1.026	881.0	1.040	1.051
18	SA-2	121 × 3.13 × 359	20	340.7	31.9	25.71	938.5	1.051	851.2	1.103	1.115
19	SA-3	121 × 3.06 × 359	30	340.7	36.7	30.03	960.4	1.076	885.2	1.085	1.081
20	SA-4	121 × 3.16 × 359	40	340.7	38.4	31.56	980.9	1.099	917.1	1.070	1.063
21	SA-5	121 × 3.20 × 359	50	340.7	35.7	29.13	945.5	1.059	896.5	1.055	1.055
22	SA-6	121 × 3.12 × 359	60	340.7	34.5	28.05	940.0	1.053	872.0	1.078	1.080
23	SA-7	121 × 3.07 × 359	70	340.7	40.7	33.56	943.6	1.057	925.8	1.019	1.008
24	SA-8	121 × 3.15 × 359	80	340.7	41.9	34.52	956.1	1.071	948.5	1.008	0.996
25	SA-9	121 × 3.13 × 359	90	340.7	39.0	32.10	972.5	1.089	923.7	1.053	1.051
26	SA-10	121 × 3.08 × 359	100	340.7	43.6	35.88	971.3	1.088	958.7	1.013	1.003
Shi et al. [12]											
27	S0-1[a]	100 × 1.74 × 401	0	335.5	42.6	35.08	569	–	539.8	1.054	1.023
28	S1-1	100 × 1.90 × 400	25	335.5	43.4	35.72	599	1.053	566	1.058	1.031
29	S1-2	100 × 1.91 × 402	25	335.5	43.4	35.72	586	1.030	566.6	1.034	1.007
30	S2-1	100 × 1.94 × 394	50	335.5	43.9	36.12	560	0.984	573.1	0.977	0.951
31	S2-2	100 × 1.96 × 397	50	335.5	43.9	36.12	581	1.021	575.8	1.009	0.982
32	S3-1	100 × 1.80 × 395	75	335.5	45.6	37.48	570	1.002	566.9	1.005	0.974
33	S3-2	100 × 1.92 × 399	75	335.5	45.6	37.48	558	0.981	581.1	0.960	0.931
34	S4-1	100 × 1.90 × 398	100	335.5	35.9	29.31	495	0.870	513.9	0.963	0.949
35	S4-2	100 × 1.90 × 400	100	335.5	35.9	29.31	528	0.928	513.9	1.027	1.012

[a] Reference stub columns with normal concrete

[b] Converted from f_{cu}

in ABAQUS for confined concrete [25]. As pointed out by Yu et al. [25], almost identical slopes of strain softening branches will be obtained if the uniaxial σ–ε curve continues to be used for concrete confined by different constant active pressures. This is against the experimental observations that the descending branch

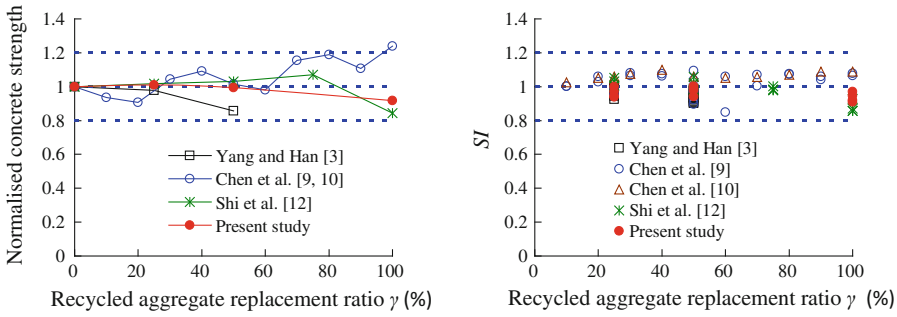

Fig. 8 Effects of γ on concrete strength and *SI* of the RACFST columns

(a) RAC **(b)** RACFST columns

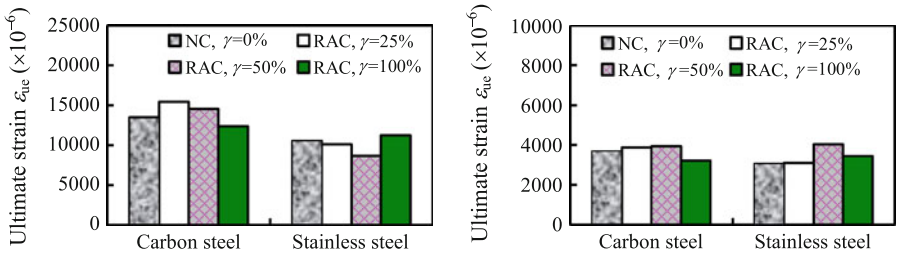

Fig. 9 Ultimate axial strains ε_{ue} of the RACFST columns

(a) Circular specimens **(b)** Rectangular specimens

becomes less steep when the confining pressure increases. Owing to the limitation of ABAQUS software, the uniaxial σ–ε curve of concrete cannot be used directly to represent the strain hardening/softening function for confined concrete. Instead, a common practice is to propose a revised σ–ε model incorporating the confining effect [25]. This σ–ε model is normally proposed based on numerical tests with parameters obtained by trial and error. Apparently, the prediction accuracy of the σ–ε model depends on the quality and quantity of test data used for the calibration.

An equivalent σ–ε relationship of confined concrete was proposed by Han et al. [26], which gives good predictions when the damage plasticity model provided in the material library of ABAQUS is used for the core concrete in the FE analysis. Han et al.'s model has been calibrated by a large amount of full-range load-deformation curves of CFST columns. The prediction accuracy of this model is generally good for normal CFST columns, thus it has been used widely. The equivalent σ–ε relationship proposed by Han et al. [26] is expressed as:

$$y = \begin{cases} 2x - x^2 & (x \le 1) \\ \dfrac{x}{\beta_0 (x-1)^{\eta} + x} & (x > 1) \end{cases} \tag{2}$$

where $x = \varepsilon/\varepsilon_0$, $y = \sigma/f'_c$; f'_c is the cylinder compressive strength of concrete; $\varepsilon_0 = \varepsilon_c + 800\xi^{0.2} \times 10^{-6}$; $\varepsilon_c = (1300 + 12.5 f'_c) \times 10^{-6}$; for circular CFST columns, $\eta = 2$, and for rectangular CFST columns, $\eta = 1.6 + 1.5/x$.

The expression for β_0 is given as below:

$$\beta_0 = \begin{cases} 0.5 \times (2.36 \times 10^{-5})^{[0.25+(\xi-0.5)^7]} (f'_c)^{0.5} & \text{and} \quad \beta_0 \ge 0.12 \quad \text{(circular CFST)} \\ \dfrac{(f'_c)^{0.1}}{1.2\sqrt{1+\xi}} \quad \text{(rectangular CFST)} \end{cases} \tag{3}$$

In the above formulae for determining ε_0 and β_0, ξ is the confinement factor used to describe the increase in plastic behaviour due to the passive confinement of the steel tube. This factor ξ is defined as $\xi = (A_s f_y / A_c f_{ck}) = \alpha(f_y/f_{ck})$, in which $\alpha = A_s/A_c$ is the steel ratio, A_s and A_c are the cross-sectional areas of the steel and core concrete respectively, f_y is the yield strength of steel, and f_{ck} is the characteristic strength of the concrete equal to $0.67 f_{cu}$ for normal strength concrete.

It should be pointed out that further research is required to accurately simulate the passive confinement provided by the steel jacket for the concrete core. Before any better confined concrete model is developed, this paper continues to use equivalent stress–strain model for confined concrete. The stress–strain model of Eq. (2) for concrete is tentatively used in this paper without considering the influence of RAC. For carbon steel, an elasto-plastic stress–strain model with five stages is used, where the detailed derivations of the stress–strain relationship can be found in Han et al. [27]. For stainless steel, a model proposed by Rasmussen [19] is used.

Shell elements S4R and solid elements C3D8R with reduced integration were employed to simulate the steel tube and concrete, respectively. A surface-based interaction between the steel tube and core concrete is used in the FE modelling [26]. In the normal direction,

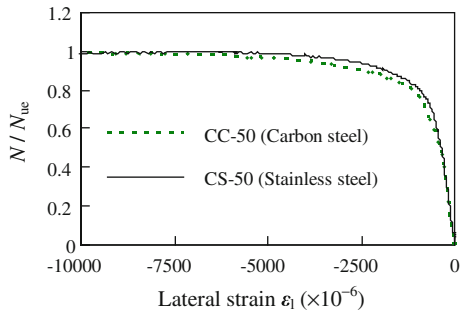

Fig. 10 Comparison of lateral strains between the carbon and stainless steel columns

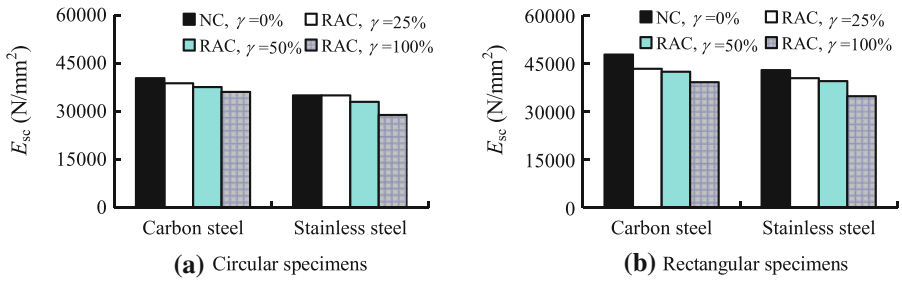

Fig. 11 Elastic moduli E_{sc} of RACFST columns

Fig. 12 The observed and predicted failure modes

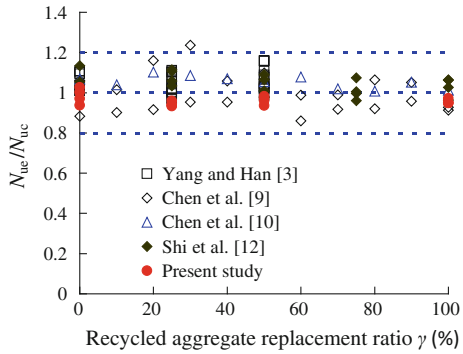

Fig. 13 Comparison between the predicted and experimental ultimate strength

a contact pressure model is adopted where the surfaces can be separated, but not allowed to penetrate each other. In the tangential direction, a Coulomb friction modelling is applied to simulate the relative slip where the friction coefficients are taken as 0.6 and 0.25 for carbon steel and stainless steel, respectively.

For the circular stub columns, no obvious lateral deflection is observed. Therefore, the initial deflection (out-of-straightness) is not considered in the FE models for these columns. For the rectangular stub columns tested in this paper, apparent lateral deformation along the minor axis develops after the peak load owing to the comparatively large slenderness along this axis. To handle this failure mode, initial deflections are considered for the rectangular columns. Therefore, an eigenvalue buckling analysis is first carried out. The deflection profile of the lowest buckling mode is then used to determine the column's initial deflections. In general, initial global imperfections (out-of-straightness) vary randomly among different supplied tubes. The range of initial global imperfections is normally from $L/500$ to $L/10{,}000$ based on the measurements reported by different researchers. A value of 1/1,000 of the member length was adopted by the Canadian and the European codes in developing steel column curves, whilst American code AISC used a probabilistically-based mean of 1/1,500 of the length [28]. In this paper, the amplitude of the initial deflection for the rectangular columns is taken as 0.6 mm ($L/1{,}000$).

Figure 12 demonstrates a comparison between the observed and predicted failure modes, which indicates a good agreement. For the rectangular column, lateral deformation can be computed after including the initial imperfections in the model. To study the influence of the overall imperfections on the behaviour of rectangular stub columns, a sensitivity analysis is carried out, where the specimen RS-100 is chosen as an example. It is found that considering the overall imperfections or not has only margin influence on the N–ε curve of this specimen. A decrease of 0.63 % in predicted ultimate strength is found when the overall

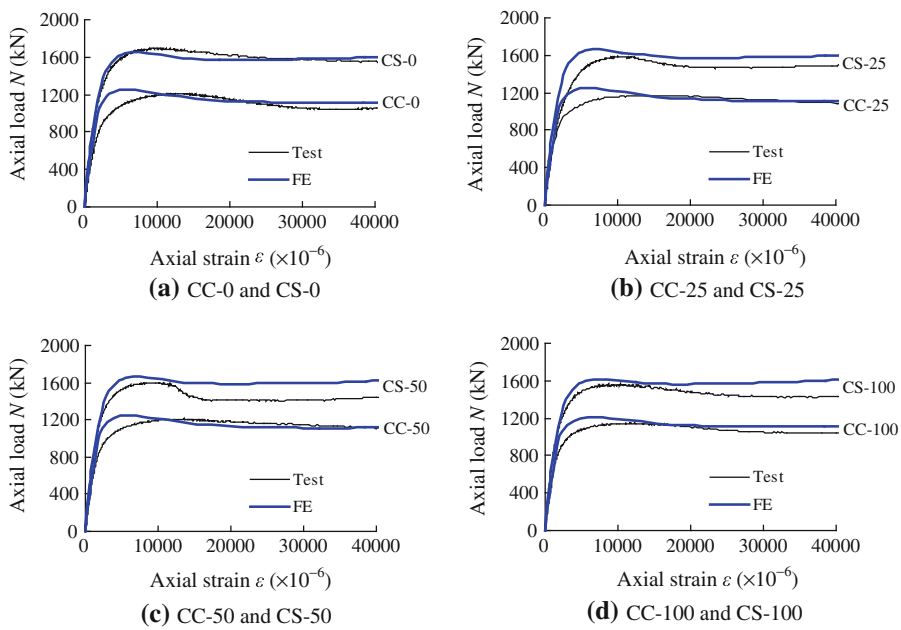

Fig. 14 Comparison between the predicted N–ε curves and current test results of circular columns

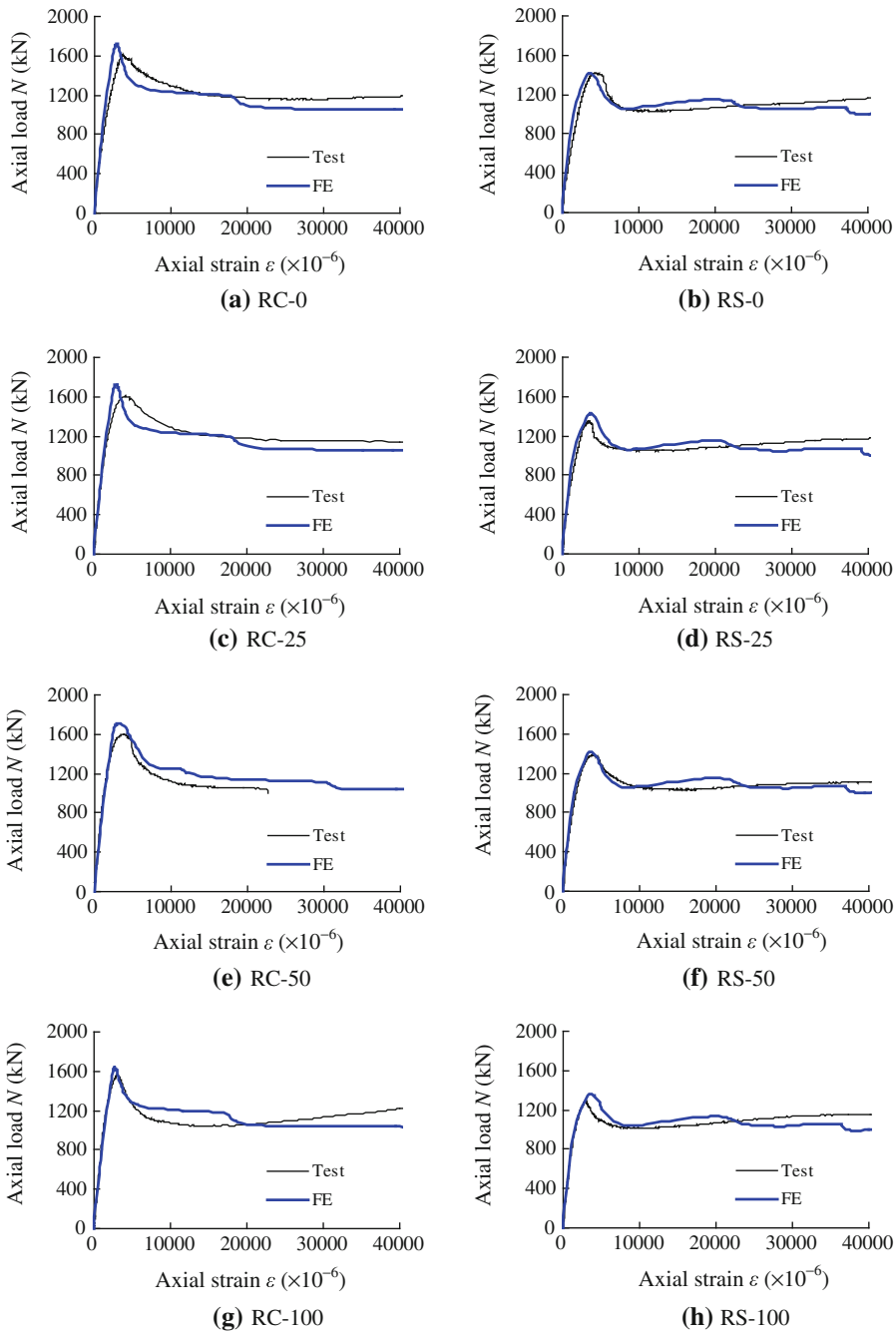

Fig. 15 Comparison between the predicted N–ε curves and current test results of rectangular columns

imperfections are taken into account. This comparison indicates that the overall imperfections have apparent influence on the failure mode of rectangular columns rather than on the ultimate strength.

Tao et al. [21] investigated the influence of initial local imperfections on the behaviour of short CFST columns. It is concluded that the influence of local imperfections is very minor and local imperfections can be generally ignored in FE simulation. This is owing to the fact that the impact of local imperfections is greatly reduced by the concrete infill, and the out-of-plane deformation of the steel tube caused by the

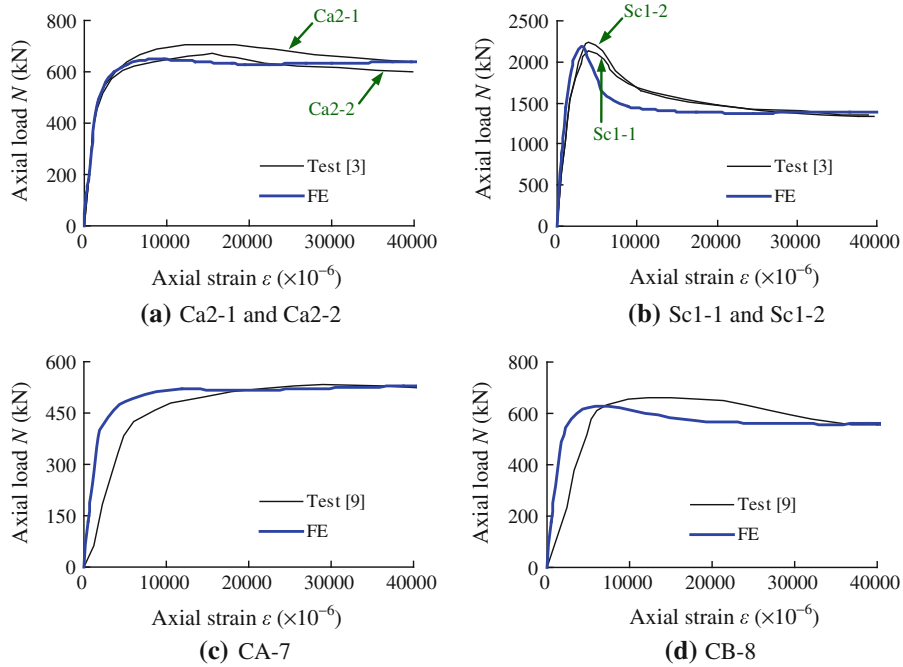

Fig. 16 Comparison between the predicted N–ε curves and independent test results

interaction stress plays a similar role as the initial imperfections [21]. Therefore, the local buckling failure mode can be simulated even without including local imperfections in the model. For this reason, local imperfections are not considered in this paper.

4.2 Predicted results

The predicted ultimate strength (N_{uc}) are given in Tables 1, 4 and 5, and compared with the experimental ultimate strength (N_{ue}) in Fig. 13. The mean value of N_{uc}/N_{ue} ratios for all the 82 RACFST stub columns is 1.021 with a standard variation of 0.069, whilst the mean value and standard variation for the 15 reference CFST columns are 1.034 and 0.068 respectively. The comparison indicates that the utilisation of RAC or not has no obvious influence on the prediction accuracy.

The predicted axial load (N) versus axial strain (ε) curves is compared with the current test results as shown in Figs. 14 and 15, whilst Fig. 16 compares the predicted N–ε curves with typical measured curves reported by others. It can be seen from Fig. 16c and d that the predicted elastic moduli for specimens presented by Chen et al. [9] are much higher than the measured values. This is mainly attributed to the fact that ε was converted directly from the measured axial shortening, which had been greatly affected by the end conditions in the initial loading stage.

From the above comparisons, it can be concluded that the predictions agree well with the test results of the RACFST stub columns. It is confirmed that the stress–strain model of concrete proposed by Han et al. [26] is still applicable to the CFST columns with RAC if the actual concrete strength of RAC is used to develop the stress–strain curves. From this, it can be inferred that the effect of RAC on the load-carrying capacity of the RACFST stub columns may not be considered, provided that the possible variation in concrete strength has been considered in the RAC mix design.

To further verify the above conclusion, Eurocode 4 is used to predict the section capacities of the test specimens listed in Tables 1, 4 and 5. The predicted values (N_{ue}/N_{EC4}) are presented in these tables. The mean value and standard variation of N_{ue}/N_{EC4} for the 82 RACFST columns are 1.001 and 0.061 respectively. Meanwhile, for the 15 reference specimens, the mean value of N_{ue}/N_{EC4} is 1.013 with a standard variation of 0.058. It can be clearly seen that Eurocode 4 gives reasonable predictions for both the RACFST columns and normal CFST.

5 Conclusions

A test program was carried out to study the behaviour of RAC filled stainless steel stub columns. A FE model developed earlier was used to predict test results reported in this paper and those presented by others. The following conclusions can be drawn from the study:

(1) The replacement of normal concrete with RAC has relatively more influence on the strength of the stainless steel composite columns than on that of carbon steel specimens.
(2) The RACFST column with stainless steel has higher residual strength than the counterpart with carbon steel.
(3) The variation in compressive strength for the RACFST columns is smaller than that for RAC with different recycled aggregate replacement ratios.
(4) A finite element model developed before for normal concrete-filled steel tubes (CFST) gives satisfactory predictions for CFST stub columns with RAC.
(5) The effect of RAC on the load-carrying capacity of CFST stub columns with RAC may not be considered, provided that the possible variation in concrete strength has been considered when using RAC.

Acknowledgments This work is supported by the Australian Research Council (ARC) under its Future Fellowships scheme (Project No: FT0991433) and National Natural Science Foundation of China (NSFC) Research Fund for International Young Scientists (Project No: 51250110074). The financial support is gratefully acknowledged.

References

1. Hansen TC (1986) Recycled aggregates and recycled aggregate concrete second state-of-the-art report developments 1945–1985. Mater Struct 19(3):201–246
2. Konno K, Sato Y, Kakuta Y, Ohira M (1997) The property of recycled concrete column encased by steel tube subjected to axial compression. Transactions of the Japan Concrete Institute 19:231–238
3. Yang YF, Han LH (2006) Compressive and flexural behaviour of recycled aggregate concrete filled steel tubes (RACFST) under short-term loadings. Steel and Composite Structures 6(3):257–284
4. Konno K, Sato Y, Ueda T, Onaga M (1998) Mechanical property of recycled concrete under lateral confinement. Transactions of the Japan Concrete Institute 20:287–292
5. Yang YF, Han LH (2006) Experimental behaviour of recycled aggregate concrete filled steel tubular columns. J Constr Steel Res 62(12):1310–1324
6. Yang YF, Han LH, Wu X (2008) Concrete shrinkage and creep in recycled aggregate concrete-filled steel tubes. Advances in Structural Engineering 11(4):383–396
7. Yang YF, Zhu LT (2009) Recycled aggregate concrete-filled steel SHS beam-columns subjected to cyclic loading. Steel and Composite Structures 9(1):19–38
8. Yang YF, Han LH, Zhu LT (2009) Experimental performance of recycled aggregate concrete-filled circular steel tubular columns subjected to cyclic flexural loadings. Advances in Structural Engineering 12(2):183–194
9. Chen ZP, Liu F, Zheng HH, Xue JY (2010) Research on bearing capacity of recycled aggregate concrete-filled circle steel tube column under axial compression loading. In: Proceedings of the International Conference on Mechanic Automation and Control Engineering, Wuhan, China, pp 1198–1201
10. Chen ZP, Chen XH, Ke XJ, Xue JY (2010) Experimental study on the mechanical behavior of recycled aggregate coarse concrete-filled square steel tube column. In: Proceedings of the International Conference on Mechanic Automation and Control Engineering. Wuhan, China, pp 1313–1316
11. Mohanraj EK, Kandasamy S, Malathy R (2011) Behaviour of steel tubular stub and slender columns filled with concrete using recycled aggregates. Journal of the South African Institution of Civil Engineering 53(2):31–38
12. Shi XS, Wang QY, Zhao XL, Collins F (2011) Strength and ductility of recycled aggregate concrete filled composite tubular stub columns. In: Incorporating Sustainable Practice in Mechanics of Structures and Materials, London, UK, pp 83–89
13. Yang YF (2011) Behaviour of recycled aggregate concrete-filled steel tubular columns under long-term sustained loads. Advances in Structural Engineering 14(2):189–206
14. Xiao J, Huang Y, Yang J, Zhang C (2012) Mechanical properties of confined recycled aggregate concrete under axial compression. Constr Build Mater 26(1):591–603
15. Etxeberria M, Vázquez E, Barra AMM (2007) Influence of amount of recycled coarse aggregates and production process on properties of recycled aggregate concrete. Cem Concr Res 37(5):735–742
16. Uy B, Tao Z, Han LH (2011) Behaviour of short and slender concrete-filled stainless steel tubular columns. J Constr Steel Res 67(3):360–378
17. Tao Z, Han LH, Wang ZB (2005) Experimental behaviour of stiffened concrete-filled thin-walled hollow steel structural (HSS) stub columns. J Constr Steel Res 61(7):962–983
18. Xiao J, Li J, Zhang C (2005) Mechanical properties of recycled aggregate concrete under uniaxial loading. Cem Concr Res 35(6):1187–1194
19. Rasmussen KJR (2003) Full-range stress-strain curves for stainless steel alloys. J Constr Steel Res 59(1):47–61
20. Yu Q, Tao Z, Wu YX (2008) Experimental behaviour of high performance concrete-filled steel tubular columns. Thin-Walled Structures 46(4):362–370
21. Tao Z, Uy B, Liao FY, Han LH (2011) Nonlinear analysis of concrete-filled square stainless steel stub columns under axial compression. J Constr Steel Res 67(11):1719–1732

22. Pryce-Jenkins V (2011) A comparative review of the latest experimental research on the use of recycled concrete aggregate in structural concretes. Department of Civil, Environmental and Geomatic Engineering, University College London, UK, Master's Dissertation
23. Belén GF, Fernando MA, Diego CL, Sindy SP (2011) Stress-strain relationship in axial compression for concrete using recycled saturated coarse aggregate. Constr Build Mater 25(5):2335–2342
24. ABAQUS (2009) ABAQUS Standard User's Manual, Version 6.9, Dassault Systèmes Corp., Providence, RI, USA
25. Yu T, Teng JG, Wong YL, Dong SL (2010) Finite element modeling of confined concrete-I: Drucker-Prager type plasticity model. Eng Struct 32(3):665–679
26. Han LH, Yao GH, Tao Z (2007) Performance of concrete-filled thin-walled steel tubes under pure torsion. Thin-Walled Structures 45(1):24–36
27. Han LH, Zhao XL, Tao Z (2001) Tests and mechanics model for concrete-filled SHS stub columns, columns and beam-columns. Steel and Composite Structures 1(1):51–74
28. Bjorhovde R (2010) Some issues for column stability criteria. In: Proceedings of the International Colloquium on Stability and Ductility of Steel Structures SDSS'Rio 2010, Rio De Janeiro, Brazil, pp 9–20